Journal of Sustainable Mining 17 (2018) 209–214

HOSTED BY

ELSEVIER

Contents lists available at ScienceDirect

Journal of Sustainable Mining

journal homepage: www.elsevier.com/locate/jsm

Research paper

The application of seismic interferometry for estimating a 1D S-wave velocity model with the use of mining induced seismicity

Rafał Czarny[a,*], Zenon Pilecki[a], Dorota Drzewińska[b]

[a] The Mineral and Energy Economy Research Institute of the Polish Academy of Sciences, Wybickiego 7A, 31-261, Krakow, Poland
[b] AGH University of Science and Technology, al. Mickiewicza 30, 30-059, Krakow, Poland

ARTICLE INFO

Keywords:
Seismic interferometry
Induced seismicity
Rayleigh surface wave
S-wave velocity
Mining terrain

ABSTRACT

The main objective of this paper is to present the usefulness of the seismic interferometry method to determine the S-wave velocity model of the rock mass affected by exploitation in the KGHM Rudna copper ore mine. The research aim was achieved on the basis of seismic data, acquired from seismograms, of 10 strong seismic events of magnitude greater than 2.6. They were recorded by a pair of seismometers deployed on mining terrain. In the first stage, the Rayleigh wave between seismometers was estimated. Then, the group velocity dispersion curves of fundamental and first higher modes were identified. Finally, inversion of the dispersion curves to a 1D S-wave velocity model up to 500 m in depth was obtained. The velocity model was determined for the part of the rock mass partially affected by mining. The results confirm similar rock mass structure and velocities of the subsurface layers as those obtained by the archival 3D model. In both models, a high degree of correlation in the boundary location between the overburden of the Cenozoic formations and the bedrock of the Triassic formations was observed. The applied methodology can be used to estimate the S-wave velocity model in other mining regions characterized by strong seismicity.

1. Introduction

Seismic velocity imaging allows the identification of the structure and properties of rock mass changed due to mining activity (Dubiński, Pilecki & Zuberek, 2000; Marcak & Zuberek, 1994; Pilecki, 2008). The changes in seismic velocity and amplitude can be used to study various processes in a geological media (e.g. Dec & Pietsch, 2012; Harba & Pilecki, 2017). Knowledge of the seismic velocity in rock mass disturbed by mining provides the possibility of evaluating the development of deformation and stress processes. These processes depend on geological and mining conditions and can lead to various types of surface deformations (Drzęźla, 1978; Popiołek, 2009; Popiołek & Pilecki, 2005). In areas of disturbed rock mass, significant stress field changes and seismicity can be observed (Dubiński & Konopko, 2000; Dubiński & Stec, 1994; Goszcz, 1989; Głowacka, 1992; Głowacka & Pilecki, 1991; Marcak & Zuberek, 1994; Mutke, Masny, & Prusek, 2016). Ground vibrations caused by strong mining tremors have a destructive impact on the structures on the terrain surface (Mutke, Chodacki, Muszynski, Kremers, & Fritschen, 2015; Tatara, 2012). Therefore, information about the development of deformation and stress processes in rock mass is important in terms of the protection of the mining area and the planning of mining works.

Seismic velocity measurements in rock mass disturbed by mining have been performed both by active and passive seismic methods (Dubiński, 1989; Gibowicz & Kijko, 1994; Hosseini, Oraee, Shahriar, & Goshtasbi, 2012, pp. 2297–2306; Marcak & Zuberek, 1994; Szreder & Barnas, 2017; Szreder, Pilecki & Kłosiński, 2008). In the last several years, the role of a new seismic interferometry method in seismic velocity measurements has been dynamically increasing (Galetti & Curtis, 2012). The cross-correlation technique, which seismic interferometry is based on, allows the estimation of the impulse response between a pair of sensors (Curtis, Gerstoft, Sato, Snieder, & Wapenaar, 2006). One of the first applications of this method in mining-related issues took place at the Garpenberg mine in Sweden at the level of underground exploitation (Olivier, Brenguier, Campillo, Lynch, & Roux, 2015a; Olivier et al., 2015b). In these studies direct S-wave and coda wave were retrieved from ambient seismic noise using the cross-correlation technique. Based on these waves, a seismic velocity model of the rock mass as well as small seismic velocity variations during a blast were estimated. Czarny, Marcak, Nakata, Pilecki, and Isakow (2016) also presented the usefulness of seismic interferometry together with ambient seismic noise registered on the surface to monitor seismic velocity changes during mining. Seismic interferometry was also the subject of the LOFRES project (Czarny et al., 2016; Isakow, Pilecki & Kubańska,

* Corresponding author.
E-mail addresses: czarny@min-pan.krakow.pl (R. Czarny), pilecki@min-pan.krakow.pl (Z. Pilecki), ddrzewinska73@gmail.com (D. Drzewińska).

https://doi.org/10.1016/j.jsm.2018.09.001
Received 8 February 2018; Received in revised form 7 May 2018; Accepted 10 September 2018
Available online 12 September 2018

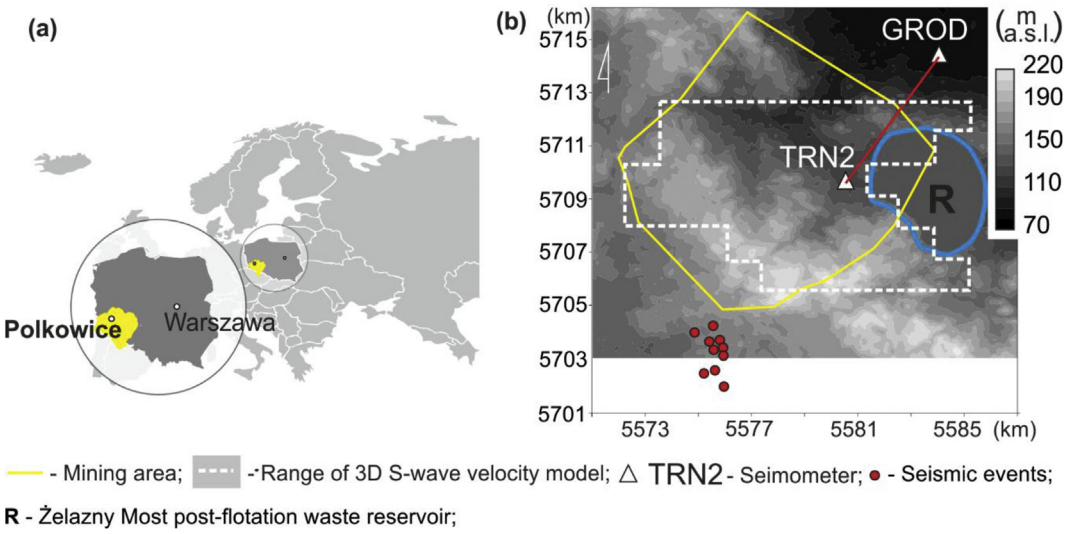

Fig. 1. (a) Location of the research area; (b) Morphology map with the location of the TRN2 and GROD seismometers in the KGHM Rudna mining area; Seismic event locations (red dots) and the range of archival 3D S-wave velocity model based on Czarny (2017) (white dashed line).

2015; Isakow, Pilecki, & Sierodzki, 2014; Krawiec & Czarny, 2017; Marcak, Pilecki & Czarny, 2014; Marcak, Pilecki, Isakow, & Czarny, 2014; Pilecki & Isakow, 2014).

The paper presents the usefulness of seismic interferometry and mining-induced seismicity to determine a 1D S-wave velocity model in the subsurface part of rock mass. The methodology of 1D model estimation is discussed. The data, consisting of ten strong seismic events, comes from the KGHM ZG Rudna mine (Fig. 1a and b). Registrations from two seismometers (TRN2 and GROD) were used in this study. The seismometers belong to the Institute of Geophysics Polish Academy of Sciences network and were deployed on the terrain surface. The calculated S-wave velocity model was compared with archival data, which is the averaged S-wave velocity model estimated with the use of seismic interferometry and ambient seismic noise (Czarny, 2017) (Fig. 1b, the area inside the white dashed line). The correspondence between the location of the geological borders in the two models and the validation of the methodology were discussed.

2. Geological and mining conditions

Geologically the mining area of the KGHM Rudna mine is located in the Fore-Sudetic monocline. The geological conditions of this region are described extensively in numerous publications (e.g. Piestrzyński, 2007; Slizowski et al., 2013). Due to the range of the velocity model which is 500 m b.t.s. The detailed description of the geology ends upon contact of the Cenozoic (overburden) deposits with the Triassic (bedrock) formations. The depth map of the Cenozoic floor is presented in Fig. 2a and based on a dataset of 100 wells (available at http://bazagis.pgi.gov.pl). The floor of the Cenozoic formations has an ordinate from approximately 230 to about 250 m above sea level (Fig. 2a).

In the overburden there are Paleogeneous deposits dated to Eocene and Oligocene, as well as Neogeneic formations dated to Miocene and Pliocene. Eocene formations include quartz and glauconitic sandstone. The thickness of the Eocene deposits is about 20 m. Above, there are Oligocene formations with a thickness of over 20 m, which is formed of quartz-glauconitic sand, quartz sand, micaceous sand, gravel and, less often, silts with an admixture of chad. In the upper part of the Oligocene formations, there is a lignite deposit called Głogów. Above the formations of the Oligocene there are Miocene formations, such as quartz gravels and quartzite gravels with a high admixture of muscovite grains, feldspar sands containing kaolin, green clays, grey clays and ash-grey clays. Miocene formations also include three lignite seams: Ścinawa, Lusatian and Henryk. Above the Miocene formations there are Pliocene formations such as: green-grey and grey-blue Poznań clays with numerous yellow and brown spots. There are also interlayers of quartz and quartz-feldspar sands. The thickness of the clays exceeds 100 m. The Quaternary formations deposited above show high lithological variability. Their thickness reaches several dozen meters. They are represented by: sands and gravels.

The copper ore deposits in the Legnica-Głogów Copper Belt has been exploited since the 1960s. The ore is extracted from a depths of 400 m–1100 m using different modifications of the room and pillar system. Measurements and theoretical calculations show that the speed of subsidence in the mining area of KGHM ZG Rudna does not exceed 1.25 mm annually (Popiołek, Hejmanowski, Krawczyk, & Perski, 2002). The maximum subsidence value in the Rudna mine is approximately 3.8 m. Subsidence isolines are shown in Fig. 2b. The shape of the isoline coincides with the exploited panels (Fig. 2b, grey fields). The Rudna mine seismic network registers a lot of strong seismic events every year (Olszewska, Lasocki & Laptokaropoulos, 2017).

3. S-wave velocity model estimation

3.1. Data and pre-processing

In order to obtain the 1D S-wave velocity model between the TRN2 and GROD seismometers (Fig. 1b), the seismic interferometry method was used. The distance between the seismometers was about 5.3 km. The source of the seismic waves was seismic events induced by mining activity (Fig. 2b, red dots). The ten seismic events were recorded between April and October 2016 by the IGF PAN network. All of the events had a magnitude greater than 2.6. Epicentres were chosen because of their locations in relation to the line connecting the seismometers. According to the phase stationarity in seismic interferometry (Snieder, 2004), the source should be located as close as possible to the extension of the line connecting the stations. The distance between the source and the nearest seismometer is also important. In this study events were about 7 km away from the TRN2 stand to avoid the problem of 'close-field' for the surface waves (Foti, Lai, Rix, & Strobbia, 2014). Distant sources from pair of receivers also reduce errors in Green's function estimation (Tsai, 2009). The seismograms were downloaded from the IS-EPOS platform which is open to the general public (www.tcs.ah-epos.eu). The analysis only includes the vertical component, which is responsible for recording the Rayleigh surface wave. Prior to cross-correlation a few pre-processing steps were performed. Firstly, the linear trend was removed and bandpass filtering in

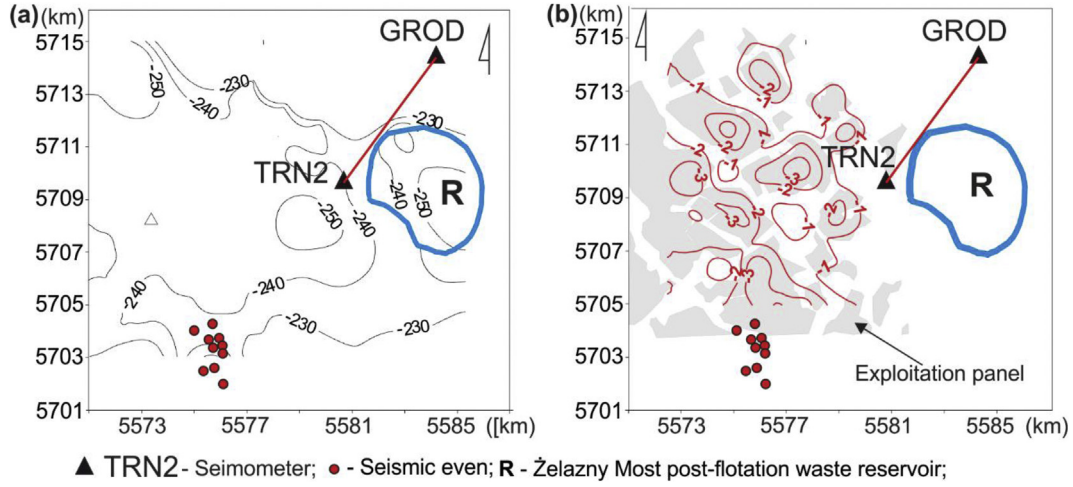

Fig. 2. (a) Depth map of the Cenozoic floor; (b) Map of subsidence and exploited panels (grey fields).

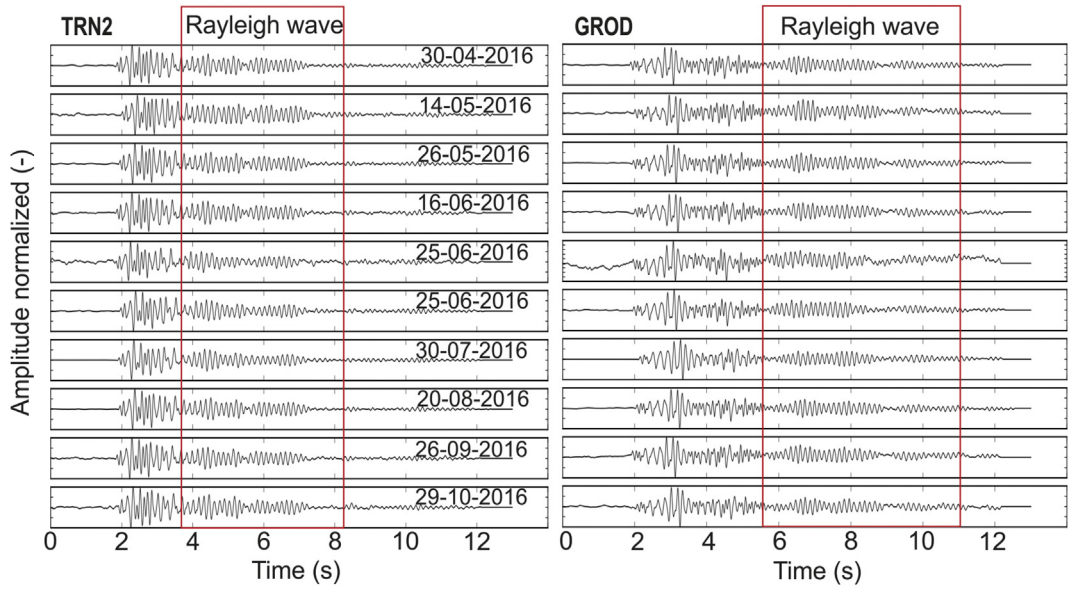

Fig. 3. Seismograms of the vertical component after pre-processing, recorded by TRN2 and GROD seismometers. The Rayleigh wave can be easily identified (red boxes).

the range from 0.05 to 2 Hz was applied. This frequency range was selected based on multiple tests to emphasize dominant seismic energy. Then, seismograms were normalized. Fig. 3 shows the result of these procedures. In the seismograms, the Rayleigh surface wave is observed on later wave arrivals (Fig. 3. seismograms inside the red box).

3.2. Cross-correlation and dispersion curve estimation

The next step in the seismic interferometry processing flow is cross-correlation. This procedure changes the seismic event source to virtual sources at the seismometer position. In this study the TRN2 seismometer was chosen as the position of the virtual source which emitted the Rayleigh wave towards the GROD seismometer. Cross-correlations were computed between seismograms from the same events. In Fig. 4 ten cross-correlation functions are presented. The negative time corresponds to the virtual source in TRN2. Amplitudes with relatively large values can be observed from 0 to about −1.5 s. They are likely associated with direct body waves. From about −2.5 s smaller amplitudes of the Rayleigh surface wave appear. The obtained correlograms were stack and subjected to the FTAN (frequency-time analysis) procedure (Dziewonski, Bloch, & Landisman, 1969) to determine the group

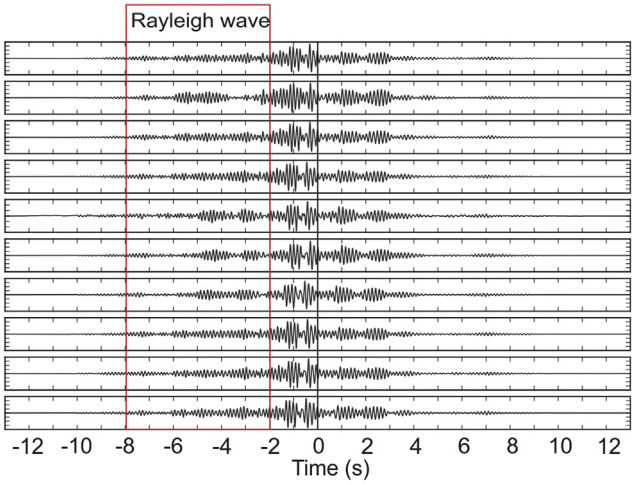

Fig. 4. The result of cross-correlation. The negative time corresponds to the estimated impulse response between the GROD and TRN2 seismometers.

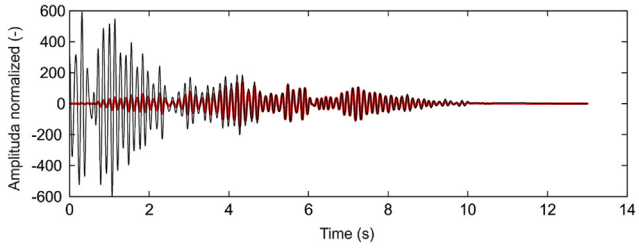

Fig. 5. The sum of 10 correlograms in the part with a negative lag time (black line). The red line indicates trace with the first 2 s tapered in order to emphasize the Rayleigh surface wave.

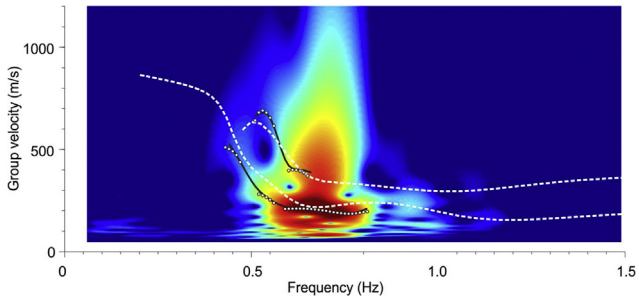

Fig. 6. The result of FTAN for Rayleigh surface wave. The white dashed lines indicate the theoretical dispersion curves of fundamental and first higher modes of Rayleigh wave from 3D S-wave model (Czarny, 2017); the white points describe empirical dispersion curves of Rayleigh wave between TRN2 and GROD; the black lines are the interpolation between the white points.

velocity dispersion curves. Prior to FTAN, the amplitudes for the first 2 s were suppressed using a cosine taper (Fig. 5). Within this time interval, surface waves were also superimposed by direct waves. Fig. 6 shows the results of FTAN. Based on the 3D S-wave velocity model (Czarny, 2017) the theoretical dispersion curves of the fundamental and first higher modes of the Rayleigh wave (white dashed lines) were calculated. The algorithm was described by Dunkin (1965) and applied by Wathelet (2008) in the Geopsy program (www.geopsy.org). The theoretical dispersion curves fit with empirical curves and were helpful with their identification. Between 0.4 and 0.8 Hz fundamental and first higher modes can be identified (Fig. 6, white points). The values between the white points have been interpolated by the spline function (Fig. 6, black line).

3.3. Inversion

The inversion of the dispersion curves to the S-wave velocity model was made through the use of the neighbourhood algorithm (Sambridge, 1999) implemented in the Geopsy program by Wathelet (2008). This algorithm uses Voronoi cells where randomly generated models with different parameters are set. For all the models theoretical dispersion curves are computed and misfits, i.e. root mean square (rms) errors, between theoretical and observed dispersion curves are determined. After each iteration new models are generated on the basis of the previous results. In this study's case the initial model includes information on the depths of the main stratigraphic boundaries. Velocities and densities for overburden and bedrock were linked with lithology. Both the fundamental and 1st higher mode were used in the inversion. After 400 iterations the best fit between the observed and theoretical curves was found with an rms error of 4.5%. Fig. 7 shows the adjustment calculated to observe the dispersion curves. In Fig. 8 the 1D S-wave velocity model after each iteration was presented.

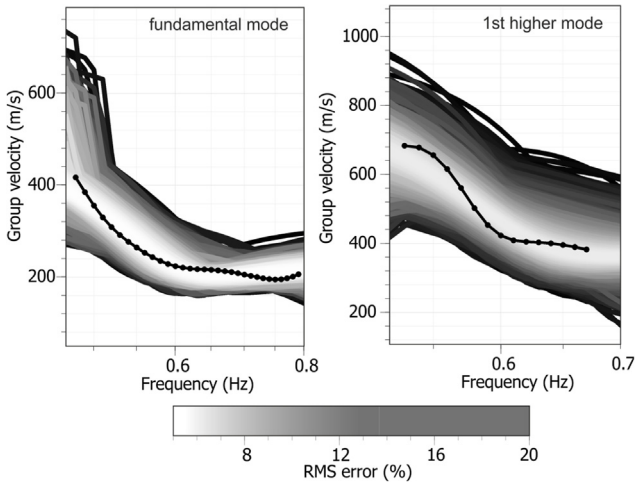

Fig. 7. Calculated (light grey lines) and observed (black line) dispersion curves for the fundamental (left) and first higher (right) modes of the Rayleigh wave.

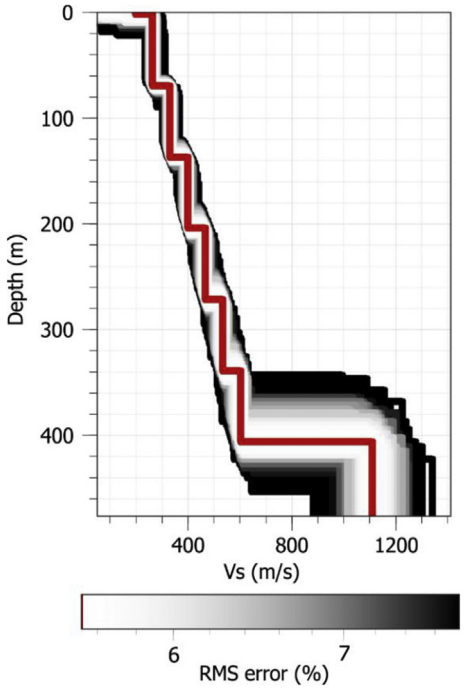

Fig. 8. Inverted S-wave velocity model. The model with the smallest RMS error is marked with the red line.

4. Discussion

The estimated 1D model, in the symmetry axis of the section between the pair of seismometers, allowed the structure and properties of the rock mass to the depth of 500 m to be imaged. In the overburden, velocities in soft layers (clays, sands and gravels) change from about 250 m/s at a depth of approximately 100 m m to about 600 m/s at a depth of 470 m. A distinct increase in S-wave velocity from approximately 600 m/s to approximately 1200 m/s is observed in the bedrock layer at the depth of about 500 m. The depth of recognition was reached due to the inversion of the fundamental and 1st higher mode in dispersive curves. Higher modes of dispersive curves are much more sensitive to deeper layer identification (Foti et al., 2014).

In Fig. 9 the estimated 1D model between seismometers TRN2 and GROD (red line – model A) is presented together with the S-wave velocity 3D model for the archived data (black dashed line with standard deviation bars – model B). Model A covers a small part of the exploited

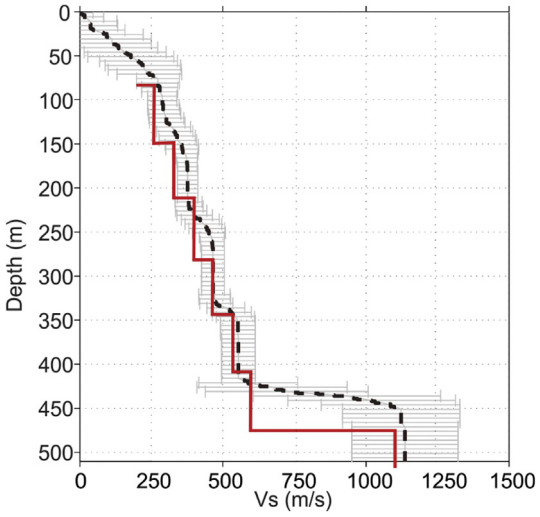

Fig. 9. S-wave velocity model between TRN2 and GROD (red line – model A) and averaged S-wave velocity (black dashed line – model B) with standard deviation for archival data (based on Czarny (2017)).

area (grey panels, Fig. 2b), therefore it refers to the fragment of rock mass affected by exploitation. Model B was estimated for almost the entire mining area of the Rudna mine (Fig. 1b, inside the white dashed line) (Czarny, 2017). Generally, both models overlap each other and they are consistent with geological data. The small differences between S-wave velocity values may be caused by the influence of local structures and the scale of the averaging of the velocity field. The boundary between Cenozoic and Triassic formations in model B is located several dozen meters higher than in model A. This is presumably related to the inclination of geological layers in the north-east direction at an angle of about 8°.

5. Conclusions

This paper presents the application of the seismic interferometry method to 1D S-wave velocity model estimation with the use of mining-induced seismicity in the mining terrain of the KGHM Rudna copper ore mine. The 1D model was estimated in the axis of symmetry of the section between two seismometers. It allows the structure and properties of rock mass to the depth of approximately 500 m to be imaged. A distinct increase in S-wave velocity is observed in the border between the overburden and the bedrock. The location of this border is consistent with the archival 3D model of S-wave velocity and geological data. The high correlation between the models and the geological data confirms that the applied methodology gave reliable results. It can be used for the preliminary recognition of structures and elastic properties of different geological media in conditions of seismic event occurrence. In particular, this methodology can be applied in the mining terrains of Polish underground hard coal and copper mines with induced seismicity. Future research can focus on the possibilities of subsidence process monitoring in mining terrain.

This methodology is cost effective and it only needs registrations from two seismometers. In comparison to seismic interferometry with seismic noise this approach involves less computational time. However, its main drawback is the fulfilment of the stationary phase, i.e. the seismometer locations depend on the location of the epicentres of seismic events.

Conflicts of interest

None declared.

Ethical statement

Authors state that the research was conducted according to ethical standards.

Acknowledgments

The paper was developed as a result of project no. PBS1/A2/12/2013 with the acronym LOFRES obtained within the 1st Competition of the Applied Research Program co-financed by the Polish National Centre for Research and Development. We thank IS-EPOS for sharing their seismological data.

References

Curtis, A., Gerstoft, P., Sato, H., Snieder, R., & Wapenaar, K. (2006). Seismic interferometry – turning noise into signal. *The Leading Edge, 25*(9), 1082–1092. https://doi.org/10.1190/1.2349814.

Czarny, R. (2017). *Ocena budowy i właściwości sprężystych górotworu metodą interferometrii sejsmicznej [Assessment of elastic properties and structure of rock mass using seismic interferometry method] (Doctoral dissertation)*Kraków: Instytut Gospodarki Surowcami Mineralnymi i Energią PAN.

Czarny, R., Marcak, H., Nakata, N., Pilecki, Z., & Isakow, Z. (2016). Monitoring velocity changes caused by underground coal mining using seismic noise. *Pure and Applied Geophysics, 173*(6), 1907–1916. https://doi.org/10.1007/s00024-015-1234-3.

Dec, J., & Pietsch, K. (2012). Możliwości sejsmicznej identyfikacji stref akumulacji gazu w utworach węglanowych cechsztynu monokliny przedsudeckiej [A possibility of seismic identification of gas accumulations in zechstein carbonate formations of the fore-sudetic monocline]. *Gospodarka Surowcami Mineralnymi-Mineral Resources Management, 28*(3), 93–112.

Drzęźla, B. (1978). *Rozwiązanie pewnego przestrzennego zadania liniowej teorii sprężystości w zastosowaniu do prognozowania deformacji górotworu pod wpływem eksploatacji górniczej wraz z oprogramowaniem [The solution of a certain spatial task of linear elasticity theory in application to the prediction of rock mass deformation influenced by mining exploitation and the software]. 90*. Zeszyty Naukowe Politechniki Śląskiej. Górnictwo.

Dubiński, J. (1989). *Sejsmiczna metoda wyprzedzającej oceny zagrożenia wstrząsami górniczymi w kopalniach węgla kamiennego [Seismic method of the advanced risk assessment of mining tremors in hard coal mines]. Prace Głównego Instytutu Górnictwa.* Seria dodatkowa, Katowice: Główny Instytut Górnictwa.

Dubiński, J., & Konopko, W. (2000). *Tąpania: Ocena, prognoza, zwalczanie [rockbursts: Assessment, forecasting and combating]*. Katowice: Główny Instytut Górnictwa.

Dubiński, J., Pilecki, Z., & Zuberek, W. (Eds.). (2000). *Badania geofizyczne w kopalniach – przeszłość, teraźniejszość i zamierzenia na przyszłość [Geophysical research in mines - past, present and future plans]*. Kraków: Wydawnictwo Instytutu Gospodarki Surowcami Mineralnymi i Energią PAN.

Dubiński, J., Stec, K., & Drzewiecki, J. (1994). Mechanizm niszczenia skał stropowych w świetle obserwacji geomechanicznych i sejsmologicznych [The mechanism of the destruction of roof rocks in the light of geomechanical and seismological observations]. *Sympozjum naukowo-techniczne tapania '94 rozwiązania inżynierskie w problematyce tąpań, ustroń 23–25 listopada 1994 r* (pp. 125–133). Katowice: Główny Instytut Górnictwa.

Dunkin, J. W. (1965). Computation of modal solutions in layered, elastic media at high frequencies. *Bulletin of the Seismological Society of America, 55*(2), 335–358.

Dziewonski, A., Bloch, S., & Landisman, M. (1969). A technique for the analysis of transient seismic signals. *Bulletin of the Seismological Society of America, 59*(1), 427–444.

Foti, S., Lai, C. G., Rix, G. J., & Strobbia, C. (2014). *Surface wave methods for near-surface site characterization.* CRC Press.

Galetti, E., & Curtis, A. (2012). Generalised receiver functions and seismic interferometry. *Tectonophysics, 532–535*, 1–26. https://doi.org/10.1016/j.tecto.2011.12.004.

Gibowicz, S. J., & Kijko, A. (1994). *An introduction to mining seismology.* Elsevier.

Goszcz, A. (1989). *Wybrane zagadnienia z problematyki wstrząsów górniczych i tąpań [Selected issues of mining tremors and rock bursts]*. Katowice: Główny Instytut Górnictwa.

Głowacka, E. (1992). Application of the extracted volume of a deposit as a measure of deformation for seismic hazard evaluation in mines. *Tectonophysics, 202*(2–4), 285–290. https://doi.org/10.1016/0040-1951(92)90114-L.

Głowacka, E., & Pilecki, Z. (1991). Seismo-acoustic anomalies and evaluation of seismic hazard at marcel coal mine. *Acta Geophysica, 39*(1), 47–59.

Harba, P., & Pilecki, Z. (2017). Assessment of time–spatial changes of shear wave velocities of flysch formation prone to mass movements by seismic interferometry with the use of ambient noise. *Landslides, 14*(3), 1225–1233. https://doi.org/10.1007/s10346-016-0779-2.

Hosseini, N., Oraee, K., Shahriar, K., & Goshtasbi, K. (2012). Passive seismic velocity tomography on longwall mining panel based on simultaneous iterative reconstructive technique (SIRT). *Journal of Central South University, 19*(8), https://doi.org/10.1007/s11771-012-1275-z.

Isakow, Z., Pilecki, Z., & Kubańska, A. (Eds.). (2015). *System LOFRES sejsmiki pasywnej z wykorzystaniem szumu sejsmicznego [LOFRES system of passive seismology with the use of seismic noise]*. Katowice: Instytut Technik Innowacyjnych EMAG.

Isakow, Z., Pilecki, Z., & Sierodzki, P. (2014). Nowoczesny system LOFRES

niskoczęstotliwościowej sejsmiki pasywnej [Modern system LOFRES for low-frequencies passive seismics]. *Przeglad Gorniczy, 70*(7), 92–96.

Krawiec, K., & Czarny, R. (2017). Comparison of an empirical S-wave velocity model and a calculated stress-strain model for a rock mass disturbed by mining. *AG 2017 – 3rd international conference on applied Geophysics, E3S web of conferences: 24*https://doi.org/10.1051/e3sconf/20172403001.

Marcak, H., Pilecki, Z., & Czarny, R. (2014a). *Interferometria sejsmiczna w zagadnieniach górniczych [Seismic interferometry in mining issues].* Kraków: Wydawnictwo IGSMiE PAN.

Marcak, H., Pilecki, Z., Isakow, Z., & Czarny, R. (2014b). Możliwości wykorzystania interferometrii sejsmicznej w górnictwie [The possibility of using seismic interferometry in mining industry]. *Przeglad Gorniczy, 70*(7), 74–83.

Marcak, H., & Zuberek, W. M. (1994). *Geofizyka górnicza [Mining geophysics].* Katowice: Śląskie Wydawnictwo Techniczne.

Mutke, G., Chodacki, J., Muszynski, L., Kremers, S., & Fritschen, R. (2015). Mining seismic instrumental intensity scale MSIIS-15 – verification in coal basins. *AIMS 2015 – fifth international symposium: Mineral resources and mine development* (pp. 551–560). RWTH Aachen University.

Mutke, G., Masny, W., & Prusek, S. (2016). Peak particle velocity as an indicator of the dynamic load exerted on the support of underground workings. *Acta Geodynamica et Geomaterialia, 13*(4), 367–378. https://doi.org/10.13168/AGG.2016.0019 184.

Olivier, G., Brenguier, F., Campillo, M., Lynch, R., & Roux, P. (2015a). Body-wave reconstruction from ambient seismic noise correlations in an underground mine. *Geophysics, 80*(3), KS11–KS25. https://doi.org/10.1190/geo2014-0299.1.

Olivier, G., Brenguier, F., Campillo, M., Roux, P., Shapiro, N. M., & Lynch, R. (2015b). Investigation of coseismic and postseismic processes using in situ measurements of seismic velocity variations in an underground mine. *Geophysical Research Letters, 42*(21), 1–9. https://doi.org/10.1002/2015GL065975.

Olszewska, D., Lasocki, S., & Leptokaropoulos, K. (2017). Non-stationarity and internal correlations of the occurrence process of mining-induced seismic events. *Acta Geophysica, 65*(3), 507–515. https://doi.org/10.1007/s11600-017-0024-y.

Piestrzyński, A. (Ed.). (2007). *Monografia KGHM polska miedź S.A. [Monograph of KGHM polska miedź S.A.] (wyd. 2). Lubin: KGHM CUPRUM sp.* z o.o. CBR.

Pilecki, Z. (2008). The role of geophysical methods in the estimation of sinkhole threat in the post-mining areas of shallow exploitation in the Upper Silesian Coal Basin, Poland. *Gospodarka Surowcami Mineralnymi-Mineral Resources Management, 24*(3/1), 27–40.

Pilecki, Z., & Isakow, Z. (2014). Projekt LOFRES – sejsmika pasywna LFS z wykorzystaniem szumu sejsmicznego [LOFRES project – low frequencies passive seismicity by use of seismic noise]. *Przeglad Gorniczy, 70*(7), 69–73.

Popiołek, E. (2009). *Ochrona terenów górniczych [Protection of mining areas].* Katowice: Wydawnictwa AGH.

Popiołek, E., Hejmanowski, R., Krawczyk, A., & Perski, Z. (2002). The application of satellite radar interferometry to the examination of the areas of mining exploitation. *Surface Mining - Braunkohle and Other Minerals, 54*, 74–82.

Popiołek, E., & Pilecki, Z. (Eds.). (2005). *Ocena przydatności do zabudowy terenów zagrożonych deformacjami nieciągłymi za pomocą metod geofizycznych [Assessment of suitability for building areas threatened with discontinuous deformations by means of geophysical methods].* Kraków: Wydawnictwo IGSMiE PAN.

Sambridge, M. (1999). Geophysical inversion with a neighbourhood algorithm – I. Searching a parameter space. *Geophysical Journal International, 138*(2), 479–494. https://doi.org/10.1046/j.1365-246X.1999.00876.x.

Slizowski, J., Pilecki, Z., Urbanczyk, K., Pilecka, E., Lankof, L., & Czarny, R. (2013). Site assessment for astroparticle detector location in evaporites of the Polkowice-Sieroszowice copper ore mine, Poland. *Advances in High Energy Physics*461764. https://doi.org/10.1155/2013/461764.

Snieder, R. (2004). Extracting the Green's function from the correlation of coda waves: A derivation based on stationary phase. *Physical Review A, 69*(4), 46610. https://doi.org/10.1103/PhysRevE.69.046610.

Szreder, Z., & Barnas, M. (2017). Assessment of the impact of an overlying coal seam edge using seismic profiling of refracted P-wave velocities. *AG 2017 – 3rd international conference on applied Geophysics, E3S web of conferences: 24*, (pp. 3001–). . https://doi.org/10.1051/e3sconf/20172401007.

Szreder, Z., Pilecki, Z., & Klosinski, J. (2008). Efektywność rozpoznania oddziaływania krawędzi eksploatacyjnych metodami profilowania tłumienia oraz prędkości fali sejsmicznej [Effectiveness of the recognition of exploitation edge influence with the help of the profiling of attenuation and the velocity of seismic wave]. *Gospodarka Surowcami Mineralnymi-Mineral Resources Management, 24*(2/3), 215–226.

Tatara, T. (2012). *Odporność dynamiczna obiektów budowlanych w warunkach wstrząsów górniczych [Dynamic resistance of building structures under mining shock conditions]. Kraków: Politechnika Krakowska im.* Tadeusza Kościuszki.

Tsai, V. C. (2009). On establishing the accuracy of noise tomography travel-time measurements in a realistic medium. *Geophysical Journal International, 178*(3), 1555–1564. https://doi.org/10.1111/j.1365-246X.2009.04239.x.

Wathelet, M. (2008). An improved neighborhood algorithm: Parameter conditions and dynamic scaling. *Geophysical Research Letters, 35*(9), 1–5. https://doi.org/10.1029/2008 GL033256.